Paraelastic properties and reorientation behavior of ⟨110⟩ off-center Ag^+ defects in RbCl and RbBr†

Rolando V. Jimenez* and Fritz Lüty
Physics Department, University of Utah, Salt Lake City, Utah 84112
(Received 29 October 1974)

The stress-induced alignment of substitutional Ag^+ defects in RbCl and RbBr was studied at low temperatures, using the uv absorption (A, D_1, and D_2 bands) of the Ag^+ defect. The elasto-optical behavior, measured under stress S of ⟨100⟩, ⟨111⟩, and ⟨110⟩ symmetry, yielded results which are in quantitative agreement with a Curie-law paraelastic behavior of ⟨110⟩ *oriented permanent elastic dipoles*. With one particular exception (which will be discussed), the three stress symmetries yield internally consistent and very precise data which test and confirm the elastic dipole model with an unprecedented accuracy. For both RbCl and RbBr systems, the E_g part of the elastic-dipole model (= level splitting under S_{100}) is found considerably larger than the T_{2g} part (or S_{111} splitting effect). These static elastic dipole properties can be used to understand the peculiar dynamic behavior of the Ag^+ defect: The high preference of reorientation by tunneling between next-nearest-neighbor (90°) instead of nearest-neighbor (60°) dipole states, can be explained by the very different way the T_{2g} and E_g elastic-dipole distortions are "dressing" and hindering these two motions. Elasto-optical measurements of the relaxation behavior as a function of stress of different symmetry yield results which agree with the predictions for one-phonon or thermally activated relaxation processes involved in the dipole reorientation.

I. INTRODUCTION

A large variety of substitutional paraelectric defects—both of the molecular and off-center point-ion type—have been discovered and studied in the cubic alkali-halide crystals during the last decade. The prominent examples of these defects have been found to have either ⟨100⟩ symmetry (like most OH^- systems[1]) or ⟨111⟩ symmetry (like the Li^+ in KCl,[2] and most CN^- systems[3]). This is a somewhat expected result if one employs the simplest possible model for a free rotor in a cubic crystal field: Using as a hindering potential the field of cubic symmetry of lowest order in terms of surface harmonics (Devonshire model),[4] one obtains a prediction of dipole states with ⟨100⟩ or ⟨111⟩ symmetry only. This model furthermore leads for large crystal potentials to an equivalence with the tight-binding model approach, in which only tunneling between nearest-neighbor dipole states is considered. This is in agreement with the experimentally verified high predominance of nearest-neighbor versus next-nearest-neighbor tunneling in all ⟨100⟩ and ⟨111⟩ dipole systems studied so far. Theoretical calculations about possible off-center defect potentials, based on more sophisticated microscopic interaction models, have so far produced predictions for ⟨111⟩ defect symmetries only (as for Li^+,[5] Ag^+ and Cu^+,[6] and for F^- defects[7]).

Irrespective of these expectations, molecular and off-center electric-dipole defects with ⟨110⟩ symmetry have been found in increasing numbers in recent years; OH^- in[1] KI and NaBr,[8] F^- in NaBr,[9] and Ag^+ in RbCl and[10] RbBr are examples. Formally a ⟨110⟩ defect orientation can be obtained in a Devonshire-like model by extending the expansion of the cubic crystal potential to the next-higher surface harmonic term V_6 and giving this term a large enough strength compared to the first order from V_4.[11] Such a ⟨110⟩ dipole model in an octahedral crystal field becomes again equivalent with a tight-binding tunneling approach, in which tunneling between nearest-neighbor ⟨110⟩ dipole states is predominant.

The electro-optical study of Ag^+ defects in RbCl and[10] RbBr revealed (besides establishing clearly the ⟨110⟩ off-center symmetry), that these defects reorient with high preference by next-nearest-neighbor (90°) tunneling compared to the (60°) nearest-neighbor process. This astonishing result deviates from the behavior found for all ⟨111⟩ and ⟨100⟩ dipoles, and from the expectation, based on octahedral-crystal-field models. We proposed earlier a hypothetical explanation of this effect,[10] which was based on the extension of the rigid-cubic-potential models, given by Pirc and Gosar[12] and Shore.[13] The strong electric and elastic coupling of the dipole with its surrounding will lead to non-cubic lattice distortions around the defect which have to be reoriented together with the dipole. This "dressing" of the dipole gives rise to strong hindering effect on the tunneling motion, which can be accounted for by a renormalization of the tunneling formalism. We proposed that the strangely inverted 90° versus 60° tunneling rates found for the Ag^+ ⟨110⟩ defect could be caused by a particular dressing effect of the dipole with elastic distortions of T_{2g} and E_g symmetry, with the latter being predominant and preventing a quick 60° reorientation. This provided the main motivation for this work: to study with elasto-optical techniques the detailed

nature of the elastic-dipole properties of Ag^+ in RbCl and RbBr.[14] The obtained results will confirm our previous explanation for the 60° and 90° reorientation, and will allow testing in general of the electric and elastic dressing model for the defect reorientation with an accuracy not achieved so far in a paraelectric-defect system.[15]

Beyond supplying a phenomenological understanding of the correlations between static and dynamic properties of this *particular* defect, we believe that the Ag^+ system supplies *the prototype behavior for essentially all molecular and off-center paraelectric systems of* ⟨110⟩ *symmetry*. Work which is in progress on various OH^- and F^- ⟨110⟩ defect systems with elasto-optical,[16] Kerr-effect,[17] and dielectric techniques[18] is yielding results which show that similar elastic-dipole effects, correlated with a particular 90° and 60° reorientation behavior, seem to be characteristic for most ⟨110⟩ paraelectric-dipole systems.

II. MODEL FOR ⟨110⟩ ELASTIC DIPOLE AND ITS ELASTO-OPTICAL BEHAVIOR

In the previous electro-optical work it was conclusively determined that the Ag^+ defect occupies the 12 possible ⟨110⟩ off-center positions [as illustrated in Fig. 1(a)], with an electric displacement-dipole-moment of 0.78 and 0.95 e Å in RbCl and RbBr, respectively. It was further clarified in this work that the three low-energy absorption bands of the Ag^+ defect (A, D_1, and D_2 bands) display a polarization behavior as indicated in Fig. 1(b): For one selected off-center dipole site (No. 3 in Fig. 1) with a particular ⟨110⟩ direction, the lowest energy (A) band is polarized parallel to the dipole axis (δ polarization), while the D_2 and D_1 bands, following at higher energies, are found polarized along the ⟨1$\bar{1}$0⟩ and ⟨001⟩ directions, respectively, i.e., along the two inequivalent directions perpendicular to the dipole axis ($\pi_{1\bar{1}0}$ and π_{001}) The electro-optical behavior, extrapolated to full field alignment, indicated, however that this polarization is not a full (100%) one, but is found empirically for all three bands to be reduced to an effective ~80% σ or π polarization. Tentative explanation for this reduced polarization behavior can be found either in a mixture of some π character into the σ transition (and vice versa), or in a small (~16°) mean deviation from the exact ⟨110⟩ orientation due to librational motion of the dipole.

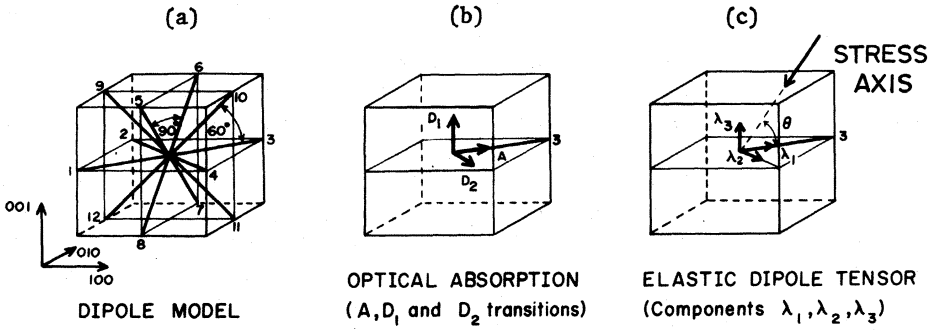

Stress axis	θ°	Energy Levels	$\alpha_i = f_i(\lambda_j)$
[100]	45° 90°	12 — $\Delta U_1 = \alpha_1 S$ — 8, 4; 60° reor.	$\alpha_1 = v_0\left(\frac{\lambda_1+\lambda_2}{2}+\lambda_3\right)$
[111]	35° 90°	12 — $\Delta U_2 = \alpha_2 S$ — 6, 6; 90° reor.	$\alpha_2 = \frac{2}{3} v_0\left(\lambda_1-\lambda_2\right)$
[110]	0° 60° 90°	12 — $\Delta U_3 = \alpha_3 S$ — 2; 60°; 90° reor. 12 — $\Delta U_4 = -\alpha_4 S$ — 8, 2; 60°	$\alpha_3 = v_0\left(\lambda_1-\lambda_2\right) = \frac{3}{2}\alpha_2$ $\alpha_4 = -\frac{1}{4} v_0\left(\lambda_1-3\lambda_2+2\lambda_3\right) = \frac{1}{2}\alpha_1 - \frac{3}{4}\alpha_2$

FIG. 1. Upper part: Illustration of the 12 equivalent sites of a ⟨110⟩ dipole, and (for a selected single-dipole state No. 3) the direction of the transition moments for the optical absorption and the directions of the components λ_1, λ_2, and λ_3 of the elastic-dipole tensor. Lower part: Energy levels for the orientational states of (classical) ⟨110⟩ dipoles under applied stress S_{100}, S_{111}, and S_{110}. Definition of the stress-splitting coefficients $\alpha_i (i=1,\ldots,4)$ and their relation to the λ_1, λ_2, λ_3 components of the elastic-dipole tensor. (v_0 is the volume per molecule).

With off-center symmetry and optical behavior already essentially clarified, we can formulate in advance the relations for the expected elasto-optical behavior of the system. The elastic-dipole properties of a ⟨110⟩ defect, as introduced by Nowick and Heller,[19] are determined by three components λ_i of the elastic-dipole strain tensor, with λ_1 in the [110] dipole axis, and λ_2 and λ_3 in the two [1$\bar{1}$0] and [001] directions perpendicular to the axis [see Fig. 1(c)]. In the table of Fig. 1 we summarize the effect of ⟨100⟩, ⟨111⟩, and ⟨110⟩ stress (S) on this ⟨110⟩ elastic-dipole system. For a ⟨100⟩ (E_g) stress, the dipole states split into a doublet of state-multiplets, with the splitting parameter α_1, determined by $\frac{1}{2}(\lambda_1+\lambda_2)-\lambda_3$ (E_g or tetragonal part of the ⟨110⟩ elastic dipole). Under S_{111} again two types of energy levels are formed, with the splitting factor α_2 determined by $\lambda_1-\lambda_2$ (T_{2g} or trigonal part of the elastic-dipole moment). For ⟨110⟩ stress a three-level system is formed from states with 0°, 60°, and 90° angle to the stress axis. While here the splitting factor α_3 between the two orthogonal dipole states is determined by the $\lambda_1-\lambda_2$ (T_{2g}) elastic-dipole part, the splitting between the 60° and 90° dipole states is given by $\lambda_1-3\lambda_2+2\lambda_3$, which can be expressed by a linear combination of the E_g and T_{2g} elastic-dipole parts ($\alpha_2=\frac{3}{2}\alpha_2$ and $\alpha_4=\frac{1}{2}\alpha_1-\frac{3}{4}\alpha_2$.) Similarly, for all other possible stress directions the splitting parameters are completely predicted by linear combinations of α_1 and α_2.

The signs of the energy splitting, i.e., the sequency of the levels in the table of Fig. 1, are determined by the sign and relative magnitude of the λ_i components, i.e., by the shape of the ⟨110⟩ defect. For $\lambda_1>\lambda_2$ and λ_3 (as assumed in Fig. 1) the elastic-dipole defect is "cigar shaped" and will align under compressive stress application into orientational states with its axis as perpendicular as possible to the applied stress. For other relations between the λ_1 components different sequences of the energy levels will be produced; in particular, the relation $(\lambda_1-\lambda_2)\gtrless 2(\lambda_2-\lambda_3)$ will decide, if for S_{110}, the 60° or 90° level is the lowest. The shape of the elastic-dipole defect, i.e., the important information about sign and relative magnitude of the λ_i (or α_i) components, has to be derived from the experiment.

In order to achieve this we make use of the fact that the elastic-dipole tensor λ_i of each defect with particular orientation [Fig. 1(c)] is directly and rigidly connected with an optical-absorption tensor, the three principal components of which are related to the A, D_1, and D_2 transitions corresponding to the σ, π_{001}, and $\pi_{1\bar{1}0}$ polarized excitations of the defect [Fig. 1(b)]. Stress-induced alignment of the elastic-dipole tensor therefore produces alignment of the optical-absorption tensor, which should be reflected in changes of the absorption strength pure zero-moment changes) for light polarized parallel (∥) and perpendicular (⊥) to the applied stress. For S_{100} and S_{111}, the optical absorption K depends only on the angle θ_i between the direction of the stress and the considered optical transition dipole:

$$K_{\parallel}\propto\sum_i n_i(S)\cos^2\theta_i,\qquad K_{\perp}\propto\sum_i n_i(S)\sin^2\theta_i, \tag{1}$$

with n_i the population of the ith dipole state. For stress in a ⟨110⟩ (or any other general) direction, the optical response perpendicular to the stress axis depends on a second angle in a polar-coordinate system too, so that one will obtain two different $K_{\perp 1}\neq K_{\perp 2}$ results. In all cases the conservation of total absorption holds:

$$\Delta K_{\parallel}=-(\Delta K_{\perp 1}+\Delta K_{\perp 2}). \tag{2}$$

Using the level-splitting and -multiplicity, summarized in Fig. 1, Boltzman statistics and the above relations, it is easy to derive the expressions for the stress-induced absorption changes $\Delta K(S)$ parallel and perpendicular to the stress (applied in ⟨100⟩, ⟨111⟩,and ⟨110⟩ direction) for optical transitions of the defect, which are fully σ, π_{001}, and $\pi_{1\bar{1}0}$ polarized. These expressions are summarized in Table I.

The expressions in Table I are written in such a way that the value for $[\Delta K(S)/K_0]_{S\to\infty}$ is factorized out, being multiplied by a function $f(\alpha_i X)$ which varies always between 0 and +1 with increasing $X=S/kT$. This allows a direct check on the sign and saturation value of the expected stress dichroism. Several general features are evident from these expressions: For S_{100}, when the dipoles order only by 60° reorientations among the three different (100) planes (but not within these planes), the stress-dichroism must be identical for the σ and $\pi_{1\bar{1}0}$ transitions. For S_{111}, on the other hand, when the dipoles order only by 90° reorientations within the three (100) planes, the stress dichroism for the σ and $\pi_{1\bar{1}0}$ transitions must be inverted in terms of parallel and perpendicular polarization, while the π_{001} transition [which sums up the dipoles in each (100) plane] should remain unchanged. For ⟨110⟩ stress with its resulting three-level system, a more complicated (and partly non-monotonous) functional behavior of the stress dichroism is expected.

The expressions listed in Table I are for transitions with a pure dipole-polarization characteristic along the σ, $\pi_{1\bar{1}0}$ and π_{001} directions. If a transition is not fully polarized but contains anisotropic unpolarized part (as was found in the electro-optical work for the Ag^+ defect), the numerical

TABLE I. Relative absorption change $\Delta K/K_0$ for light polarized parallel (∥) and perpendicular (⊥) to a stress S applied in ⟨100⟩, ⟨111⟩, and ⟨110⟩ direction, calculated for a ⟨110⟩ elastic dipole with σ, π_{110}, and π_{001} polarized optical transitions, as a function of $X=S/kT$.

		σ polarization (A band)	$\pi_{1\bar{1}0}$ polarization (D_2 band)	π_{001} polarization (D_1 band)
S_{100}	$\frac{\Delta K_\parallel}{K_0}$	$(-1)\,\frac{1-e^{-\alpha_1 X}}{1+2e^{-\alpha_1 X}}$	$(-1)\,\frac{1-e^{-\alpha_1 X}}{1+2e^{-\alpha_1 X}}$	$(+2)\,\frac{1-e^{-\alpha_1 X}}{1+2e^{-\alpha_1 X}}$
	$\frac{\Delta K_\perp}{K_0}$	$(+\frac{1}{2})\,\frac{1-e^{-\alpha_1 X}}{1+2e^{-\alpha_1 X}}$	$(+\frac{1}{2})\,\frac{1-e^{-\alpha_1 X}}{1+2e^{-\alpha_1 X}}$	$(-1)\,\frac{1-e^{-\alpha_1 X}}{1+2e^{-\alpha_1 X}}$
S_{111}	$\frac{\Delta K_\parallel}{K_0}$	$(-1)\,\frac{1-e^{-\alpha_2 X}}{1+e^{-\alpha_2 X}}$	$(+1)\,\frac{1-e^{-\alpha_2 X}}{1+e^{-\alpha_2 X}}$	0
	$\frac{\Delta K_\perp}{K_0}$	$(+\frac{1}{2})\,\frac{1-e^{-\alpha_2 X}}{1+e^{-\alpha_2 X}}$	$(-\frac{1}{2})\,\frac{1-e^{-\alpha_2 X}}{1+e^{-\alpha_2 X}}$	0
S_{110}	$\frac{\Delta K_\parallel}{K_0}$	$(-\frac{1}{4})\,\frac{4-8e^{-\alpha_3 X}+4e^{\alpha_4 X}}{1+e^{-\alpha_3 X}+4e^{\alpha_4 X}}$	$(-\frac{1}{4})\,\frac{4e^{-\alpha_3 X}-8-4e^{\alpha_4 X}}{e^{-\alpha_3 X}+1+4e^{\alpha_4 X}}$	$(+\frac{1}{2})\,\frac{4e^{\alpha_4 X}-2-2e^{-\alpha_3 X}}{4e^{\alpha_4 X}+1+e^{-\alpha_3 X}}$
	$\frac{\Delta K_{1\bar{1}0}}{K_0}$	$(-\frac{1}{4})\,\frac{4e^{-\alpha_3 X}-8+4e^{\alpha_4 X}}{e^{-\alpha_3 X}+1+4e^{\alpha_4 X}}$	$(-\frac{1}{4})\,\frac{4-8e^{-\alpha_3 X}+4e^{\alpha_4 X}}{1+e^{-\alpha_3 X}+4e^{\alpha_4 X}}$	$(+\frac{1}{2})\,\frac{4e^{\alpha_4 X}-2-2e^{-\alpha_3 X}}{4e^{\alpha_4 X}+1+e^{-\alpha_3 X}}$
	$\frac{\Delta K_{1001}}{K_0}$	$(+\frac{1}{2})\,\frac{4e^{\alpha_4 X}-2e^{-\alpha_3 X}-2}{4e^{\alpha_4 X}+e^{-\alpha_3 X}+1}$	$(+\frac{1}{2})\,\frac{4e^{\alpha_4 X}-2e^{-\alpha_3 X}-2}{4e^{\alpha_4 X}+e^{-\alpha_3 X}+1}$	$(-1)\,\frac{4e^{\alpha_4 X}-2-2e^{-\alpha_3 X}}{4e^{\alpha_4 X}+1+e^{-\alpha_3 X}}$

saturation values $\Delta K(\infty)/K_0$ in Table I will be reduced by an effective reduction factor δ without a change in the form of the subsequent $f(\alpha_i X)$ functions. Thus for the experiments the stress-splitting coefficients α_i and this reduction factor δ will be regarded as adjustable parameters.

III. CRYSTAL PREPARATION AND EXPERIMENTAL TECHNIQUES

The RbCl : Ag^+ and RbBr : Ag^+ crystals were grown by the Kyropoulos method in an inert argon atmosphere from ultrapure material, with added amounts of AgCl (4×10^{-4}) and AgBr (8×10^{-4}) to the corresponding rubidium-halide melt. Properly oriented samples were cut and polished with typical dimensions 7–8 mm in the stress direction, 2–3 mm for the optical path, and 4–5 mm in the third direction.

Silver ions in rubidium halides tend to form aggregates at higher temperatures, with this tendency markedly increasing under anion variation $Cl^- \rightarrow Br^- \rightarrow I^-$ of the host lattice. As an example, RbBr:Ag^+ crystals after their growth and slow cooling process display a broad and partly unstructured Ag^+ aggregate spectrum (Fig. 2, dashed line). Quenching from 600 °C transforms this spectrum into the A-, D_2-, and D_1-band-spectrum characteristic for the atomic Ag^+ center (Fig. 2, full curve). In this quenched form the crystals were used for the measurements. When keeping the crystals over extended periods at room temperature, the A, D_2, and D_1 bands decrease and the broad silver-aggregate spectrum reappears (Fig. 2, curves 3 and 4).

A stainless-steel rod in the exchange-gas cryostat allowed the transmission of pressure from an air-expended bellows on the top of the cryostat to the sample. The stress applied to the crystal was determined (from the manometer reading) by the geometrical factor of the arrangement. The validity of the latter was carefully checked by measurements of the photoelastic effect in a test crystal, using an optical compensator.

The absorption measurements were done in a

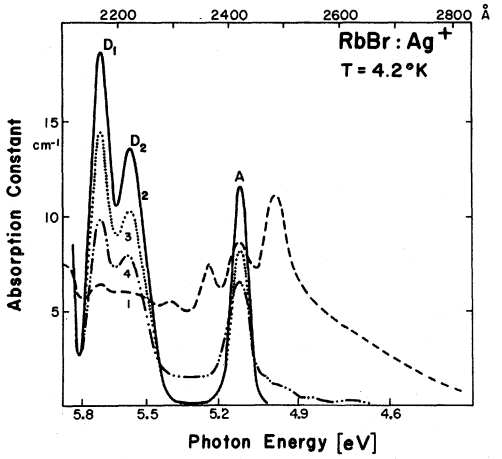

FIG. 2. Absorption spectrum of Ag^+ in RbBr, measured at 4.2 °K: (a) after slow thermal annealing from ~600 °C; (b) after quenching of crystal from ~600 °C to room temperature; (c) after keeping quenched sample at room temperature for 2 weeks; (d) after keeping quenched sample at room temperature for 4 months.

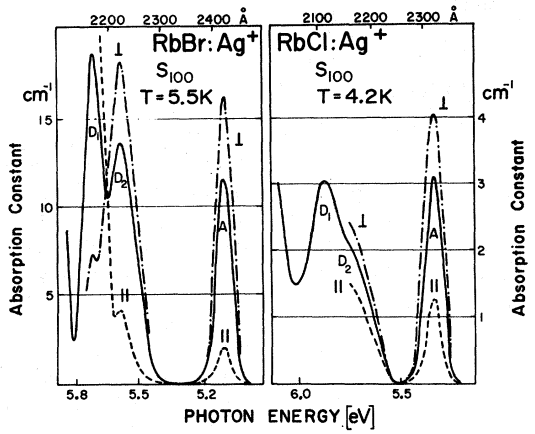

FIG. 3. Low-temperature absorption spectra of Ag^+ ions in RbBr and RbCl, measured without stress (full curve), and under ⟨100⟩ stress application with polarization either parallel (dashed curve) or perpendicular (dash-dotted curve) to S_{100}. The applied stress is 300 and 140 atm for the RbBr : Ag^+ and RbCl : Ag^+ system, respectively.

Cary 14 spectrophotometer with an inserted uv glan prism. The reproducibility of the stress-optical results for different samples was better than 5%.

IV. EXPERIMENTAL RESULTS

A. Static behavior of stress dichroism

Figures 3 and 4 summarize several absorption spectra obtained at low temperatures for RbBr : Ag^+ (left-hand side) and RbCl : Ag^+ (right-hand side). The full line represents in all cases the Ag^+ absorption spectrum in the absence of applied stress, displaying the well-resolved low-energy A band and the partially overlapping D_1 and D_2 bands (which are better separated in RbBr compared to RbCl). Stress application (of the indicated magnitude) leads to very pronounced spectral changes, represented by the dashed and dashed-dotted curve for polarization parallel and perpendicular to the stress, respectively. While ⟨100⟩ stress (Fig. 3), leads to the same dichroism in the $A(\sigma)$ and $D_2(\pi_{1\bar{1}0})$ bands, ⟨111⟩ stress (Fig. 4) yields a stress dichroism for these two bands, inverted in sign, and no stress-dichroism for the $D_1(\pi_{001})$ band—all in agreement with the predictions in Table I. The measured stress-induced absorption changes in these (and all other) measurements were found within experimental accuracy to be pure changes of the absorption strength (zero-moment changes) without noticable changes of the position and width of the bands. Thus the basis for the pure reorientation dichroism, developed in Sec. II, is experimentally well established, and we can from now on represent the stress-induced dichroism for each band by a single value $K(S)/K(0)$, the absorption strength of the band under stress $K(S)$, normalized to its value in the absence of stress $K(0)$. This quantity is related to the $\Delta K(S)/K(0)$ expressions in Table I by

$$K(S)/K(0) = 1 + \Delta K(S)/K(0).$$

Figure 5 shows for both Ag^+ systems the $K(S)/K(0)$ behavior of the A and D_2 bands, measured as a function of an applied S_{100} stress at different temperatures and plotted against S/T. As expected for the paraelastic alignment model (Table I), the A- and D_2-band dichroism measured at different temperatures, coincide for this plot into a single curve each for parallel and perpendicular polarization. Compared to the saturation value $K(\infty)/K(0)$ expected for fully polarized optical transitions (1.5 and 0 for perpendicular and parallel polarization, respectively), the actual observed values are found somewhat reduced. An excellent fit to the S_{100} expression in Table I can be obtained (full curve in Fig. 4) by choice of an effective reduction factor $\delta = 0.85$ for the ΔK effect, and a stress-splitting coefficient α_i for both systems as indicated in the figure caption.

Figure 6 shows the same type of measurement for both Ag^+ systems under ⟨111⟩ stress. In order to achieve a single curve for the A- and D_2-band dichroism this time, the measured dichroism for the two bands has to be plotted inverted in terms of the sign of the ΔK effect. As in Fig. 4, the expected saturation values for $S \to \infty$ (1.5 and 0) are not quite reached experimentally. The observed A- and D_2-band $K(S)$ behavior can be fitted with the expressions in Table I by use of the same reduction factor 0.85, used in Fig. 4, and the α_2-splitting coefficients indicated in the figure.

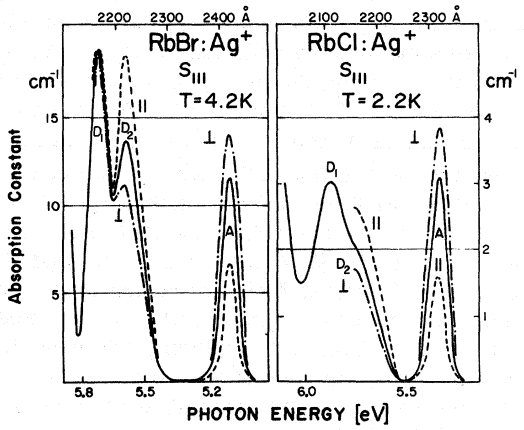

FIG. 4. Low-temperature absorption spectra of Ag^+ ions in RbBr and RbCl, measured without stress (full curve), and under ⟨111⟩ stress application with polarization either parallel (dashed curve) or perpendicular (dash-dotted curve) to S_{111}. The applied stress is 180 and 200 atm for the RbBr : Ag^+ and RbCl : Ag^+ system, respectively.

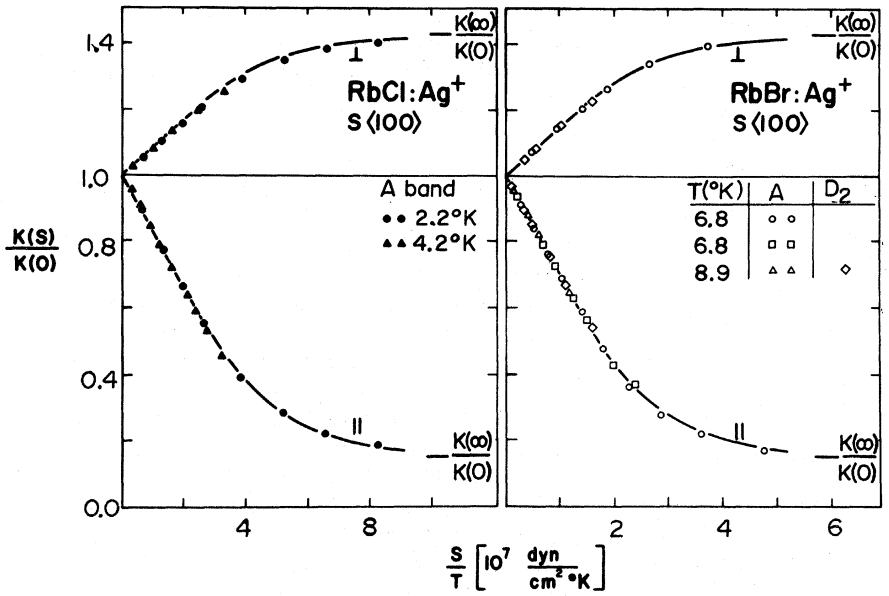

FIG. 5. Relative absorption strength $K(S)/K(0)$ for the A and D_2 band of Ag^+ in RbCl and RbBr under applied ⟨100⟩ stress, measured at various low temperatures and plotted as a function of S/T. The full line has been calculated, using $\alpha_1 = 0.83\times10^{-23}$ cm^3 for RbCl : Ag^+ and $\alpha_1 = 1.46\times10^{-23}$ cm^3 for RbBr : Ag^+.

For stress applied in a ⟨110⟩ direction, we have a situation, as illustrated in the insert of Fig. 7, with three dipole levels X, Y, and Z. For the σ-polarized A-band transition, dipole state X will absorb only light polarized parallel to S_{110}, dipole state Y only light polarized perpendicular to S in $[1\bar{1}0]$, while dipole state Z will absorb light of all three polarizations. The actual measurement in Fig. 7 for the A band in RbCl:Ag^+ clearly indicates depopulation of the dipole levels X and Y by the stress, and alignment into the dipole state Z. Therefore the relative energy positions of the three levels must be as given in the insert of Fig. 7, with level Z (dipoles with 60° angle to S_{110}) lying below level Y (dipoles with 90° angle to S_{110}). An excellent quantitative fit (full curves) to all three measurements can be obtained with the S_{110} expressions from Table I, using the previously-employed reduction factor $\delta = 0.85$ for the ΔK effect, and the two splitting parameters α_3 and α_4 given in Fig. 7.

For the just treated RbCl : Ag^+ system under S_{110}, the 60° and the 90° reorientation processes among dipole levels X, Y, and Z (see insert in Fig. 7) occur with time constants of 10^{-2} and 10^{-5} sec, respectively, so that both relaxations appear instantaneously and are inseparable in our experiment. For the RbBr : Ag^+ system, however, the 60° reorientation is completely frozen in below ~5 °K (with $\tau > 10^3$ sec) so that at low temperatures only the 90° relaxation process ($\tau \approx 10$ sec) between dipole levels X and Y should occur. This is indeed experimentally verified by the measurements in Fig. 8 for the RbBr : Ag^+ system under S_{110} at 4.2 °K. The A- and D_2-band dichroism for parallel and perpendicular polarization shows a pure 1 : 1 population exchange between dipole levels X and Y, while the absence of any D_2-band dichroism and any absorption change in the perpendicular [001] direction directly indicates the absence of any relaxation into dipole level Z. The measured behavior in Fig. 8 can be fitted with the appropriate expressions for the two-level (X and Y) system, using again the reduction factor $\delta = 0.85$ and the splitting parameter α_3 given in the figure.

At somewhat higher temperatures (> 5 °K), the previously frozen in 60° relaxation becomes effective in RbBr : Ag^+ so that a S_{110} experiment in this range should produce full 60° and 90° relaxation among all dipole levels X, Y, and Z. Stress application at 6.5 °K (where $\tau_{60°} \approx 0.3$ sec) and subsequent measurement at 4.2 °K (Fig. 9) indeed produces a stress dichroism markedly different from the one produced by S_{110} at 4.2 °K (Fig. 8) and qualitatively similar to that of the corresponding RbCl : Ag^+ case in Fig. 7. As the α_3-splitting parameter for the S_{110} case has been already determined by the partial-relaxation experiment in Fig. 8, it should no longer be regarded as a free-fitting parameter. Using this same α_3 value and the previously employed reduction factor $\delta = 0.85$ for the dichroism, a good fit to the S_{110} expressions from Table I for full dipole relaxation can be achieved (full curve in Fig. 9) by choice of the parameter α_4 given in the figure. In order to test this latter case (RbBr : Ag^+ under S_{110}) further, the temperature variation of the stress dichroism was measured, using light polarization in [001] perpendicular to S_{110}. A plot of the measured initial slopes of the $K(S)$ curves versus the inverse temperature yields a straight line, as expected for paraelastic alignment behavior (Fig. 10), A fit of this curve

with the expression from Table I (using again the previously determined α_3 value), yields an α_4 valued 0.14×10^{-23} cm^3 in good agreement with the value derived from the S_{110} stress-variation measurement in Fig. 9 (0.18×10^{-23} cm^3).

B. Dynamic behavior of stress dichroism

For Ag^+ in RbCl, the two low-temperature relaxation times for 90° and 60° reorientation were found by electro-optical techniques to have values of about 10^{-5} and 10^{-2} sec, respectively.[10] In agreement with this, all changes of the stress dichroism in our experiments appeared "instantaneously" compared with the time constant ($\geq 10^{-1}$ sec) of the optical instrument.

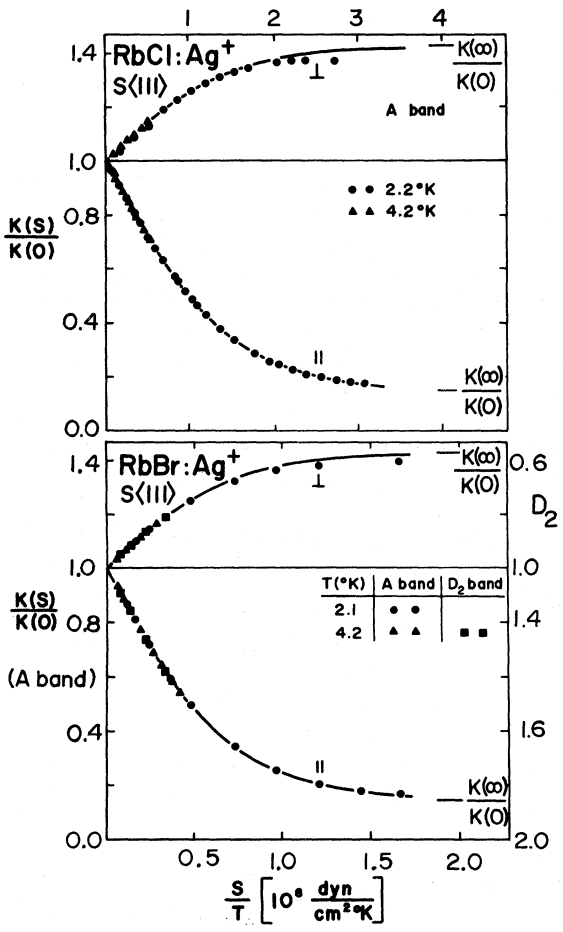

FIG. 6. Relative absorption strength $K(S)/K(0)$ for the A and D_2 band of Ag^+ in RbCl and RbBr under applied ⟨111⟩ stress, measured at various low temperatures and plotted as a function of S/T. The full line has been calculated, using $\alpha_2 = 0.19\times10^{-23}$ cm^3 for RbCl : Ag^+ and 0.39×10^{-23} cm^3 for RbBr : Ag^+. [Note the different $K(S)/K(0)$ scale on the left- and right-hand side of the lower figure, applicable to the A and D_2 band measurements, respectively, and the different S/T scale for the upper and lower figure.]

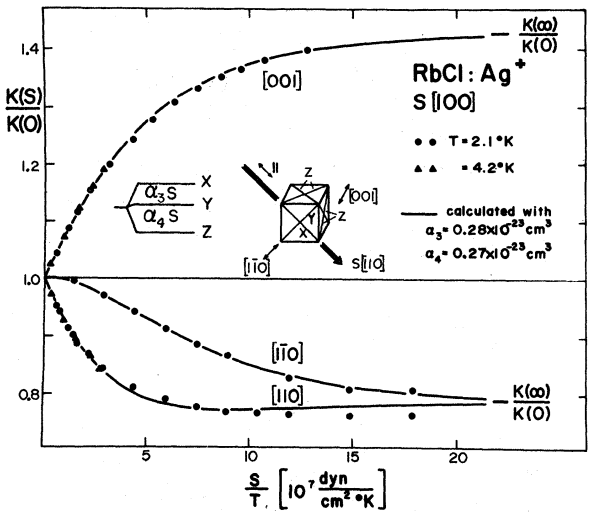

FIG. 7. Relative absorption strength $K(S)/K(0)$ of the A band in RbCl, measured at two low temperatures under S_{110} application with light polarized parallel to S[110], and in the two inequivalent directions perpendicular to the stress [110] and [001], plotted as a function of S/T. The full curves are calculated using the stress-splitting coefficients α_3 and α_4 given in the figure. (The insert illustrates the geometry of the three dipole states X, Y, and Z under S_{110} and their level splitting.)

The RbBr:Ag^+ system, however, with its much slower low-temperature relaxation behavior, allowed a direct monitoring of the time-dependent stress dichroism after a quick change of the applied-stress conditions. Figure 11 summarizes some typical original curves from an extended set of time-dependent stress-dichroism measurements. It shows how the optical absorption of the A band

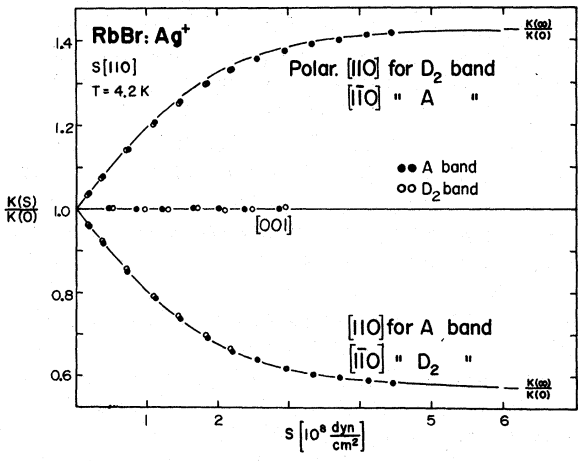

FIG. 8. Relative absorption strength of the A and D_2 band in RbBr, measured under S_{110} application for three light polarization at 4.2°K (where only 90° reorientation occurs). The full curves are calculated with the stress-splitting coefficient $\alpha_3 = 0.59\times10^{-23}$ cm^3.

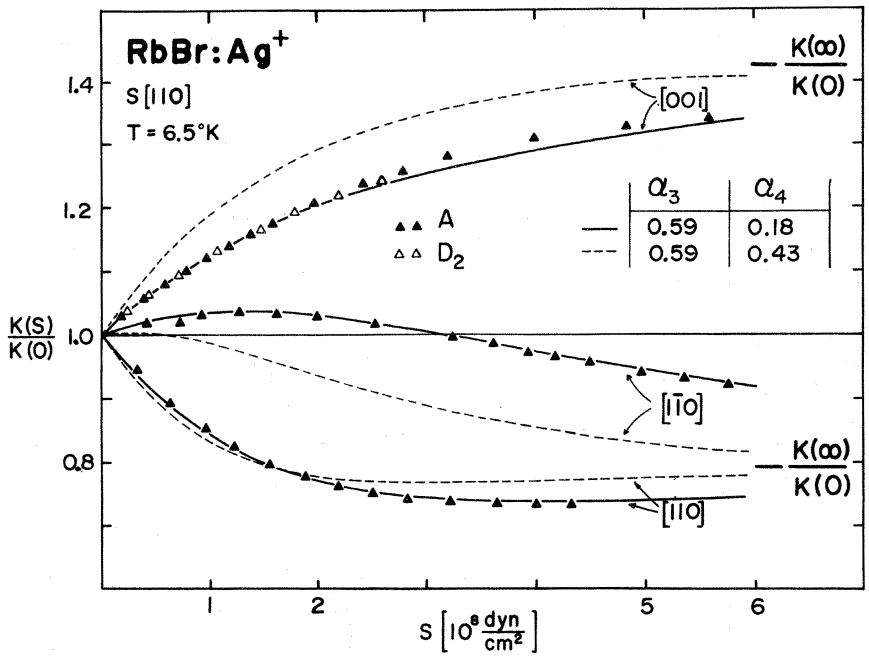

FIG. 9. Relative absorption strength of the A and D_2 band in RbBr measured under S_{110} application for three light polarizations at 6.5 °K (where both 90° and 60° reorientation occurs). The full and dashed curves are calculated with the α_3 and α_4 values (in units 10^{-23} cm^3) given in the figure.

(measured parallel to S) behaves in time under a sudden application and removal of both a small (25 atm) and large (200 atm) uniaxial stress of ⟨100⟩, ⟨111⟩, and ⟨110⟩ symmetry. The S_{111} and S_{110} measurement performed at 2 °K (where only the quick 90° reorientation process takes place) yield a relaxation time of about 10 sec, in good agreement with the electro-optical determined value.

For the S ⟨100⟩ case, the slow 60° reorientation appears only at higher temperatures, with a relaxation time of several minutes at ~5 °K under small stress splitting. As can be seen in Fig. 11, this relaxation process shows a drastically increased rate after the application of large (200 atm) stress, while removal of this large stress leads again to a relaxation (under $S=0$) of the original slow rate.

The results of systematic relaxation experiments of the type in Fig. 11 are summarized in Figs. 12–14. In Fig. 12, the measured 90° relaxation rate as a function of stress (normalized to its value at $S=0$) is plotted versus $(\alpha S/2kT)_{T=\text{const}}$ for S_{111} and S_{110} at 2.0 and 1.7 °K, respectively. In both cases a similar gradual decreases of the relaxation time with stress is observed. A much more drastic reduction of the relaxation time (already apparent in the time-dependent curves in Fig. 11) appears under S ⟨100⟩ for the slow 60° reorientation process, as shown in a normalized semilogarithmic plot in Fig. 13. For 4.9° the reduction of the initial relaxation time $\tau(0)$ under stress was measured up to ~400 atm [where $\tau(S)$ becomes comparable to the time constant of the optical instrument]. In order to follow the $\tau(S)$ dependence further to higher stress amplitudes, the temperature was reduced to 4.2 °K. At this temperature the relaxation process is more than an order of magnitude slower [$\tau(0)\approx 10^4$ sec], so that it becomes detectable with reasonable rates only for large applied stress ($S>400$ atm). The measured 4.2 °K data in the high-stress regime were normalized into the $\tau(S)/\tau(0)$ plot of Fig. 13 by assuming that its stress dependence in the low-stress regime is the same as the one measured for 4.9 °K. With this normalization we obtain from the composite data of both temperatures a normalized $\tau(S)/\tau(0)$ dependence, which displays an approximate ex-

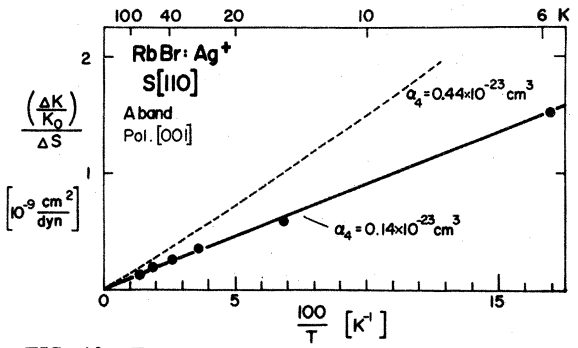

FIG. 10. Temperature dependence of the initial slope of the stress-alignment curves $\Delta K/\Delta S$, measured for RbBr:Ag$^+$ under S_{110} in the A band for a polarization [001] to the stress, and plotted in an inverse temperature scale. The fitting of the data with the expected model behavior (Table I) yields a splitting parameter $\alpha_4 = 0.14 \times 10^{-23}$ cm^3.

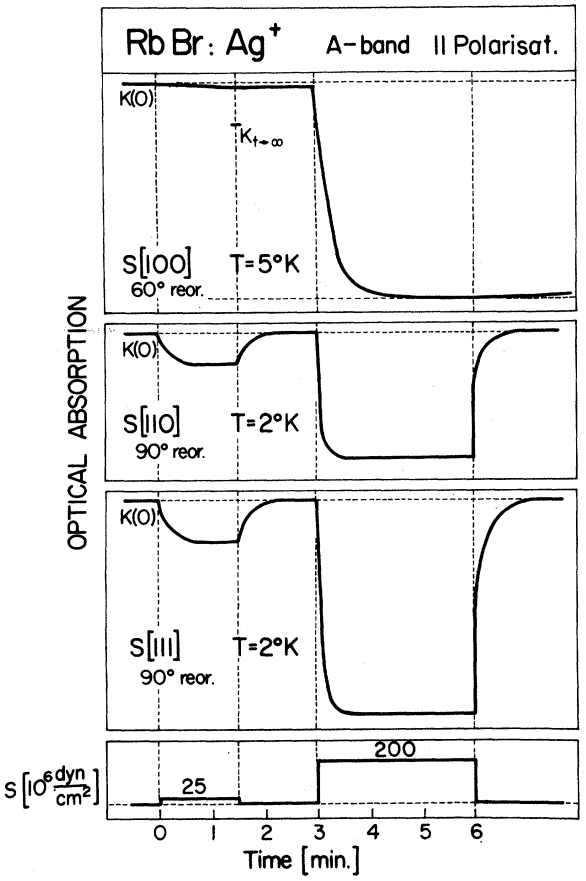

FIG. 11. Time dependence of the (parallel polarized) A-band absorption of Ag^+ in RbBr, measured under sudden application of a small (25 atm) and large (200 atm) uniaxial stress of ⟨100⟩, ⟨111⟩, ⟨110⟩ symmetry. (For the ⟨100⟩ small-stress application case the final equilibrium value $K(S)_{t\to\infty}$ is indicated which would be achieved after a long enough time.)

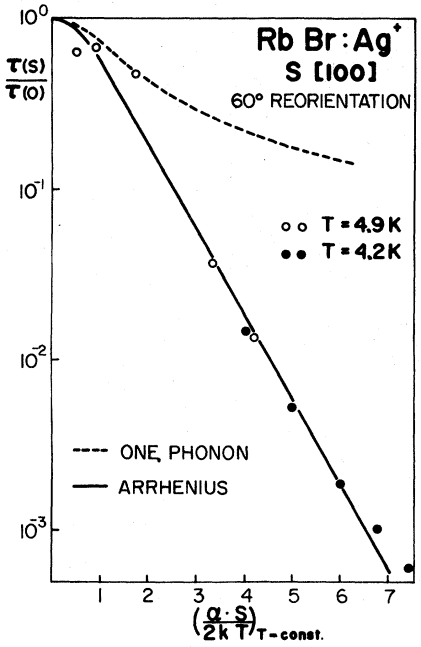

FIG. 13. Semilogarithmic plot of the normalized relaxation time $\tau(S)/\tau(0)$ as a function of stress S_{100} for RbBr : Ag^+, measured at two different temperatures and plotted (in a normalized way) versus $\alpha S/2kT$. The used α value is the one determined by the static S_{100} experiment. The full curve is calculated for Arrhenius process, the dotted curve for one-phonon relaxation.

ponential decay of the relaxation time by more than three orders of magnitude under ⟨100⟩ stress up to 800 atm.

Finally, Fig. 14 shows the $\tau(S)$ behavior of the 60° orientation process under applied ⟨110⟩ stress, yielding a much weaker $\tau(S)$ dependence compared to the S_{100} case in Fig. 13.

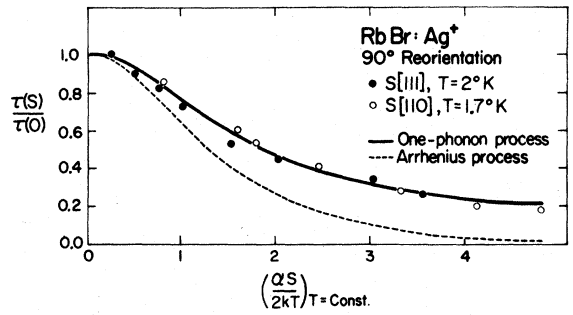

FIG. 12. Normalized relaxation time $\tau(S)/\tau(0)$ as a function of the stress S_{111} and S_{110}, plotted (each for constant temperature) as a function of $(\alpha S/2kT)$. The splitting parameters α used for S_{111} and S_{110} are the values determined for the static S_{111} and S_{110} experiments. The full curve is calculated for one-phonon relaxation, the dotted curve for an Arrhenius process.

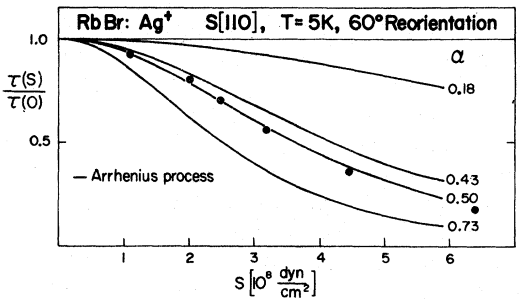

FIG. 14. Normalized stress dependence $\tau(S)/\tau(0)$ of the slow 60° relaxation process, measured in RbBr : Ar^+ at 5 °K in the A band with a [001] polarization to the stress S [110]. The full curves show the calculated behavior for an Arrhenius process, using various α parameters (in units 10^{-23} cm^3).

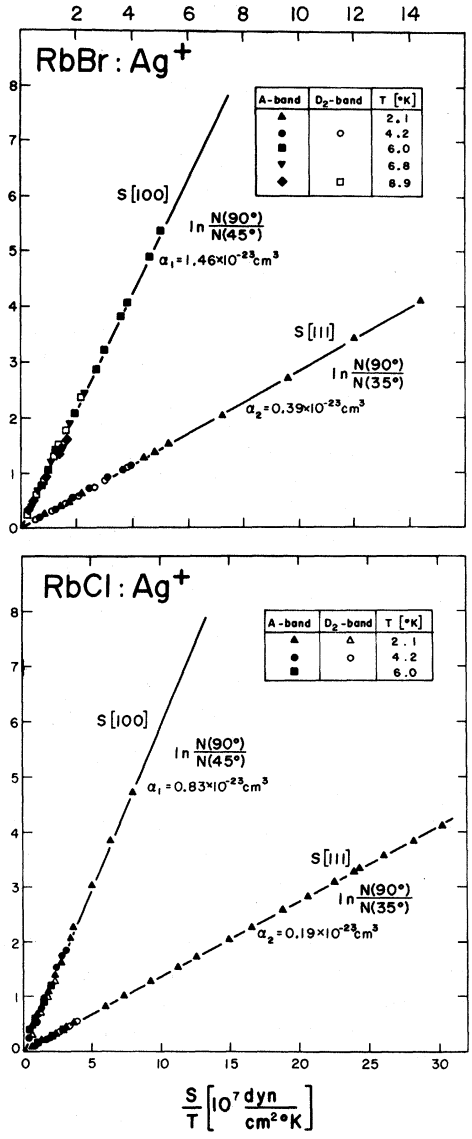

FIG. 15. Summary of all S_{100} and S_{111} experiments in the A and D_2 band of Ag^+ in RbCl and RbBr performed at various low temperatures. The logarithmic population ratio of the two-level-system under S_{100} and S_{111}, as derived from these optical measurements, is plotted as a function of S/T.

V. DISCUSSION

A. Static-paraelastic-alignment behavior

In all measured cases, S_{100}, S_{111} and S_{110}, the observed S/T dependence of the zero-moment changes of the A, D_1, and D_2 bands could be quantitatively fitted to the calculated expressions for a ⟨110⟩ elastic dipole with permanent anisotropic-optical-transition moments. This establishes beyond any doubt the ⟨110⟩ symmetry of the elastic dipole—in agreement with the ⟨110⟩ electric-dipole symmetry derived from the electro-optical work. Furthermore, the assignment of a σ, $\pi_{1\bar{1}0}$, and π_{001} polarization to the A, D_2, and D_1 band, respectively, is exactly the same as the one derived from the electro-optical work. A quantitative fit of the dichroism curves into the saturation region, however, needed for both the field and stress alignment the assumption of a somewhat reduced ΔK effect compared to the expectation for fully polarized transitions. This effective reduction factor (which was similarly found to be necessary to account for the field and stress-induced uv dichroism of OH^- dipoles) was determined in the electro-optical work[10] as 0.80 ± 0.05, and in the elasto-optical work as 0.85 ± 0.02 (the latter value being somewhat more accurate due to the more complete stress alignment). Thus both field- and stress-alignment measurements come exactly to the same conclusion on the ⟨110⟩ dipole symmetry and the assignment of the A, D_2 and D_1 bands as optical transitions with ~84% σ, $\pi_{1\bar{1}0}$, and π_{001} dipole-polarization character.

Figure 15 summarizes in comprehensive form the results of the independent S_{100} and S_{111} experiments in both systems performed in the A and D_2 bands at various temperatures.[20] Using an assumed 85% optical polarization character of these transitions and the expressions in Table I, the logarithmic population ratio of the two-level system under S_{100} and S_{111} was calculated for all measured optical transitions, stress and temperature values, and plotted against S/T. As expected for the paraelastic-alignment model, the data for each substance and stress-symmetry coincide into a perfect straight-line dependence through the origin, yielding by their slopes the α_1 and α_2 parameters. The most significant and clear result for both RbCl : Ag^+ and RbBr : Ag^+ systems is the fact that the tetragonal (E_g) elastic-dipole part (given by α_1) is considerably larger than the T_{2g} part (determined by α_2).[21]

These α_1 and α_2 values, derived directly and independently from the S_{100} and S_{111} experiments, should predict—within the elastic-dipole model—unambiguously the level splitting for any alternative stress symmetry. Thus our third experiment, with ⟨110⟩ stress, is a critical test on the validity and internal consistency of the elastic-dipole model used. In Table II we compare the splitting values α_3 and α_4, measured in the S_{110} experiment, with the values predicted from the S_{100} and S_{111} splitting parameters α_1 and α_2 by the relations $\alpha_3 = \frac{3}{2}\alpha_2$ and $\alpha_4 = \frac{1}{2}\alpha_1 - \frac{3}{4}\alpha_2$. We note the following:

(i) For the RbCl : Ag^+ system under S_{110}, both measured α_3 and α_4 parameters agree exactly with the predicted values. The measured S_{110} stress dichroism (Fig. 7) can be quantitatively fitted by calculated curves using α_3 and α_4 values predicted

TABLE II. Stress-splitting coefficients α_3 and α_4, as measured directly by the S_{110} experiment, and as determined indirectly from the S_{100} and S_{111} data, using the relations $\alpha_3=\frac{3}{2}\alpha_2$ and $\alpha_4=\frac{1}{2}\alpha_1-\frac{3}{4}\alpha_2$.

	RbCl : Ag^+		RbBr : Ag^+	
	$\alpha_3(10^{-23}\ cm^3)$	$\alpha_4(10^{-23}\ cm^3)$	$\alpha_3(10^{-23}\ cm^3)$	$\alpha_4(10^{-23}\ cm^3)$
From S_{110}	0.28	0.27	0.59	0.16
From S_{111}	0.28		0.59	
From $S_{100}+S_{111}$		0.27		0.44

from the S_{100} and S_{111} experiment (full curves in Fig. 7).

(ii) For the RbBr : Ag^+ system under S_{110}, the splitting effects α_3 and α_4 can be separated due to the different 60° and 90° reorientation rates: (a) At 2 °K where only the 90° reorientation between the two higher levels (split by α_3) takes place, the measured stress dichroism (Fig. 8) agrees perfectly with the calculated behavior, using $\alpha_3=\frac{3}{2}\alpha_2$. (b) At higher temperatures, where both 60° and 90° reorientations occur under S_{110}, the stress dependence of the dichroism at 5 °K yields a value of $\alpha_4=0.18\times10^{-23}$ cm^3 (Fig. 9), while the $1/T$ temperature variation of the dichroism yields $\alpha_4=0.14\times10^{-23}$ cm^3 (Fig. 10). The mean value $\alpha_4=0.16\times10^{-23}$ of these (several times carefully repeated) experiments is in severe disagreement with the predicted value

$$\alpha_4=\tfrac{1}{2}\alpha_1-\tfrac{3}{4}\alpha_2=0.43\times10^{-23}\ \text{cm}^3.$$

Thus for both the α_3 and α_4 value in RbCl : Ag^+ and for α_3 in RbBr : Ag^+ we find a quantitative agreement, which verifies the validity and internal consistency of the elastic-dipole concept with an accuracy which so far has not been obtained experimentally.[22]

This quantitative agreement, which establishes confidence in the elastic-dipole concept and in our experimental method, makes it necessary, on the other hand, to take the disagreement for the singular case of α_4 in RbBr:Ag^+ very seriously. Both the stress dependence of the dichroism (measured in three inequivalent polarization directions with internally consistent results, Fig. 9) and the $1/T$ temperature dependence (Fig. 10) yield a result which deviates far outside any possible experimental error from the predicted behavior (comparison of full and dashed curves in Figs. 9 and 10). We will return to this serious discrepancy with the elastic-dipole concept later.

B. Stress dependence of the relaxation behavior

In all cases investigated (Figs. 12–14), a decrease of the relaxation time τ with the applied stress was observed, with the amount of the reduction depending on the stress symmetry. Similar variations of the relaxation under splitting ΔU of the dipole levels has been observed previously for paraelastic O_2^- defects[23] and for electric-field splitting of OH^- and Ag^+ defects.[1,10] Two different relaxation models have been discussed for the interpretation of these $\tau(\Delta U)$ effects:

(a) *One-phonon-assisted tunneling.* The relaxation time τ of a two-level system, split by an energy difference $\Delta U=\alpha S$, should vary with the stress (at a fixed temperature T) like[10]

$$\tau(S)/\tau(0)=(2kT/\alpha S\tanh(\alpha S/2kT). \tag{3}$$

(b) *Classical-rate (Arrhenius process).* The stress dependence of τ for a two-level system at a fixed temperature should be

$$\tau(S)/\tau(0)=[\cosh(\alpha S/2kT)]^{-1}. \tag{4}$$

In Fig. 12 both these functions are plotted, using the α_2 and α_3 splitting parameters from the static S_{111} and S_{110} experiment for the S_{111} and S_{110} data, respectively. We note the following:

(i) When using the—measured and expected—ratio between the S_{111} and S_{110} splitting parameters $\alpha_3:\alpha_2=\frac{3}{2}$, the plotted $\tau(S)$ dependence for S_{111} and S_{110} in Fig. 12 become identical. This is a further independent confirmation for the validity of the relation $\alpha_3=\frac{3}{2}\alpha_2$.

(ii) Using the measured absolute values for α_2 and α_3, the $\tau(S)/\tau(0)$ dependence for the 90° reorientation process fits accurately the calculated behavior for the one-phonon process. This agrees fully with the result obtained for RbBr : Ag^+ under an E_{111} electric-field splitting, where the $\tau(E)/\tau(0)$ dependence was found to follow similarly the one-phonon relaxation behavior.

It must be noted that the temperature variation of the 90° reorientation process, measured electro-optically, does not reflect a one-phonon relaxation as clearly as the field and stress dependence would imply. While at high temperatures $T>5$ °K the exponential dependence of τ on the inverse temperature indicates a classical-rate process, the onset of a much weaker temperature variation below 5 °K shows that tunneling becomes predominant. The temperature variation of τ, however, never becomes the T^{-1} dependence expected for a one-phonon process, but has a higher power T dependence

(about $\tau \propto \tau^{-2.5}$ at 2 °K). This may indicate that multi-phonon contributions to the relaxation process can not be neglected in this temperature range.

Aside from this last unexplained side feature, the quick 90° reorientation process shows consistent results under S_{111}, S_{110}, and E_{111} splitting which indicate basically a one-phonon relaxation process.

This S_{111} and S_{110} result is in striking contrast to the one obtained under S_{110} for the stress dependence of the slow 60° reorientation process. The observed very large $\tau(S)$ variation (of more than three orders of magnitude) plotted semilogarithmically in Fig. 13, follows—after some deviations in the small-stress regime—an exponential behavior for large stress. The gross feature of this behavior can be well fitted with the $[\cosh(\alpha S/2kT)]^{-1}$ law for an Arrhenius process, using the α_1 splitting factor from the S_{100} static experiment. [A one-phonon relaxation would produce the much weaker $\tau(S)$ variation, indicated by the dashed line in Fig. 13.]

This result is in agreement with the exponential $1/T$ dependence of the 60° relaxation process, measured electro-optically. Thus both temperature and splitting dependence of τ give evidence for a classical thermally activated process (with a barrier height of $\Delta U \approx 160$ °K).

The third case, the slow 60° reorientation under S_{110} at higher temperatures, is more complicated because three levels are involved in the relaxation process. The two upper levels are connected by the quick 90° relaxation and can therefore be regarded for our purpose to be "instantaneously" in thermal Boltzmann equilibrium at all times. Both these levels, in turn, are connected to the lowest level by the slow 60° reorientation, and it is this latter process which we measure in its $\tau(S)$ dependence in Fig. 14. While for small splitting the relaxation is a composite process within this three-level system, for large stress (when basically full alignment of the upper subsystem is achieved by the quick 90° process) the 60° relaxation into the lowest state becomes essentially that of a two-level system, with a separation of $\alpha_4 S_{110}$. As the 60° reorientation is a classical-rate process, the $\tau(S)_{110}$ dependence for large stress should therefore approach the calculated $[\cosh(\alpha S/2kT)]^{-1}$ behavior with $\alpha = \alpha_4$. We indicate in Fig. 14 several such calculated curves with different α parameters: (i) $\alpha = 0.73 \times 10^{-23}$ cm^3 (which would be the splitting of the lowest level from the average of the two upper ones); (ii) $\alpha = 0.43 \times 10^{-23}$ cm^3, which would be the splitting between the two lowest level α_4, predicted by the elastic-dipole relation $\alpha_4 = \frac{1}{2}\alpha_1 - \frac{3}{4}\alpha_2$; (iii) $\alpha = 0.18 \times 10^{-23}$ cm^3, the effective α_4 splitting obtained in the static S_{110} experiment (which disagreed with the elastic-dipole model).

The observed $\tau(S)$ dependence definitely discards the latter value, yielding a best fit to an effective splitting value of $\alpha = 0.5 \times 10^{-23}$ cm^3, close to the α_4 value expected from the elastic-dipole relation $\alpha_4 = \frac{1}{2}\alpha_1 - \frac{3}{4}\alpha_2$. Thus the discrepancy of α_4 with the elastic-dipole model, showing up in the static S_{110} experiment, does not appear in the dynamic $\tau(S)$ behavior.

C. Elastic-dipole dressing and reorientation motion

We now examine the interrelation between the elastic-dipole properties of the Ag^+ defect and its 60° and 90° reorientation behavior, which is illustrated in Fig. 16. Due to the elastic-dipole character of the defect (i.e., its nonspherical shape or elastic interaction with the surrounding) a defect of given orientation is surrounded by noncubic lattice distortions. [The cubic (A_{1g}) part of these distortions is not affected by the reorientation and will not be considered.] These elastic distortions, illustrated in Fig. 16 for the nearest neighbors of a dipole with a particular ⟨110⟩ orientation under (a), consist of two components of E_g and T_{2g} symmetry, as illustrated under (b) and (c). The

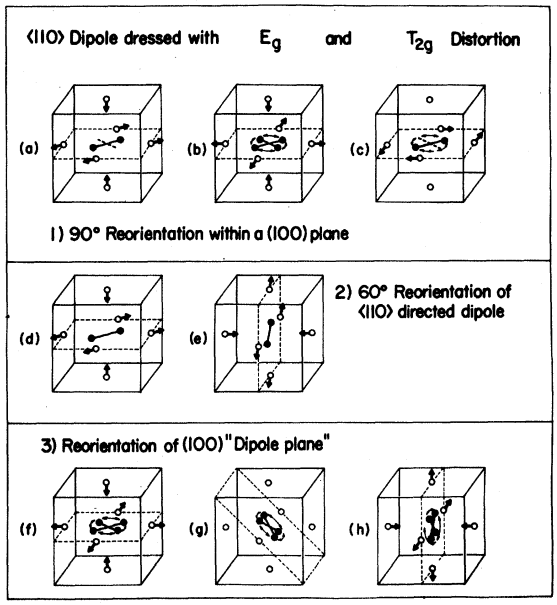

FIG. 16. Schematic illustrations of the elastic-dipole dressing and its effects on the reorientation of a ⟨100⟩ elastic dipole. (1) One particular ⟨110⟩ dipole state and its nearest neighbor distortions due to elastic interactions (a), which consist of a component of E_g and T_{2g} symmetry (b) and (c). Dipole reorientation within the indicated (100) plane by 90° jumps reorients the T_{2g} but not the E_g distortion. (2) One particular ⟨110⟩ dipole state with its elastic distortions, before and after a 60° reorientation process: Both E_g and T_{2g} distortions take part in the reorientation. (3) (100) "dipole plane" (with a rapidly rotating ⟨110⟩ defect), dressed with an E_g distortion, and its reorientation into another (100) plane. Only the E_g dressing will affect this reorientational motion.

strength of these two elastic-dipole components are directly measured by the experimentally determined stress-splitting coefficients:

$$E_g \text{ part: } \alpha_1 = v_0[\tfrac{1}{2}(\lambda_1+\lambda_2)+\lambda_3],$$

$$T_{2g} \text{ part: } \alpha_3 = \tfrac{3}{2}\alpha_2 = v_0(\lambda_1-\lambda_2),$$

with v_0 the molecular volume and λ_i the strain components of the elastic dipole tensor, defined in their direction in Fig. 1(c). A defect of given orientation is "dressed" by these elastic distortions, and in the reorientation process both the dipole and these distortions have to be reoriented. Pirc and Gosar[12] and Shore[13] have shown for the case of reorientation by tunneling that the effective tunneling matrix element Δ of the system (defect + distortions) is composed of the tunneling matrix element Δ^0 of the "naked" dipole in a (hypothetical) rigid cubic lattice surrounding, multiplied by a dressing or renormalization factor which contains in an exponential way the elastic-dipole components which take part in—and therefore hinder—the rotational motion of the defect. A more detailed account of this dressed tunneling mechanism, which resembles the polaron motion of electrons, is given in the following paper.[15]

It is evident [see Fig. 16(a)–(c)] that the 90° reorientation of a ⟨110⟩ defect within a particular (100) plane leaves the E_g distortion unchanged and rotates only the T_{2g} component. The 90° tunneling is therefore dressed or hindered only by the T_{2g} ($=\alpha_2$) elastic-dipole part, with an effective tunneling matrix element of

$$\Delta^2_{90°} = \Delta^2_0 e^{c_1\alpha_2^2}.$$

This situation is different for the 60° reorientation of a ⟨110⟩-directed dipole [illustrated in Figs. 16 (d) and (e)] in which both the E_g and T_{2g} parts of the elastic dipole rotate and thus contribute to the exponential renormalization factor of the tunneling matrix element.

There is an alternative way to look at the second type of reorientation (60° process) illustrated under No. 3 in Fig. 16. The quick 90° reorientational motion of the Ag^+ defect among the subset of four states in a (100) plane, defines in a certain way a new planar defect, a pancake-shaped (100) elastic-dipole disk, characterized by the E_g distortion and carrying no electric-dipole moment. Reorientation of this (100)-oriented dipole plane could occur as indicated in Figs. 16(e)–(g), so that this motion is dressed or hindered only by the E_g elastic-dipole part. In this picture our "60° dipole reorientation" would be in fact a "90° reorientation of the dipole plane."[24]

Whatever the exact nature of the second reorientation process, it is evident that its dressing or renormalization factor contains the E_g elastic-dipole part, while the 90° reorientation contains only the T_{2g} part. We found in this work that the E_g component is large compared to the T_{2g} component. This confirms qualitatively our previous explanation for the particular two-fold motional behavior: *The slow rate of the* 60° *motion is brought about by a strong dressing or hindering effect from a large* E_g *distortion, while the quick* 90° *tunneling is only relatively little hindered by the smaller* T_{2g} *distortions*. For a quantitative analysis, the constants c_i in the renormalization factors $e^{-c_i\alpha_j}$ must be known. In the following paper[15] these c_i values are determined from shell-model calculations for various alkali-halides and coupling mechanisms. It will then be shown that these computed c_i and the experimentally determined α_j values (together with the electric-dipole moment) give a consistent explanation for the experimentally observed 60° and 90° reorientation behavior within the dressed tunneling model.

In spite of this success in explaining the dynamic tunneling behavior from static defect properties, several important questions are left unanswered. Only for RbCl : Ag^+ are both 90° and 60° reorientations really tunneling motions. For RbBr : Ag^+ only the quick 90° process is based on tunneling (below 5 °K), while the 60° rotation is always a classical process; for $T > 5$ °K both motions in RbBr : Ag^+ become thermally activated processes with a rate τ^{-1} (determined from the temperature dependence) of

$$\tau_{60}^{-1} = 2\times10^{11}\ \text{sec}^{-1}\times\exp-(161\ °\text{K}/T),$$

$$\tau_{90}^{-1} = 2\times10^{9}\ \text{sec}^{-1}\times\exp-(87\ °\text{K}/T).$$

While the strong exponential dependence on the E_g and T_{2g} elastic dressing was able to explain the large difference for 60° and 90° reorientation for the case of the *quantum motion*, it is not clear why this difference prevails in the regime of *classical motion* too, showing up now as a factor of 2 difference in the activation energy.

A dressing by elastic distortions (or a changed effective moment of inertia I*) should enter into the description of a classical thermally activated process only very weakly by a change of the attempt frequency ($\nu \propto I^{*-1/2}$) which could never produce the large difference in the classical rates. Besides this, the attempt frequency for the 60° process (derived from the measured exponential relaxation behavior)[10] is found two orders of magnitude *higher* than that of the 90° process; the preference for the latter process at low temperatures arrives apparently from its lower activation energy.

It would be very desirable if the concepts developed for the dressed tunneling motion could be extended into the regime of reorientation by thermally activated processes. The Ag^+ system in RbCl and RbBr provide borderline cases for classical and

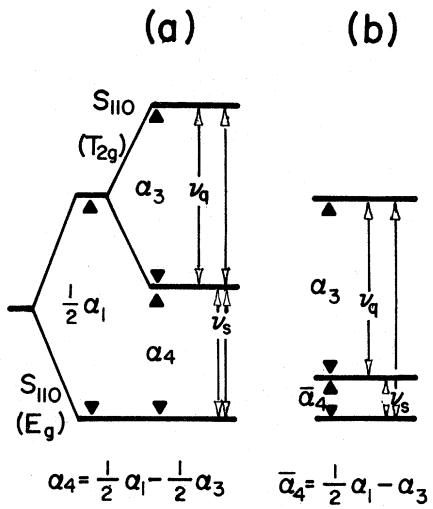

FIG. 17. Illustration of the α_4 discrepancy for RbBr : Ag^+. (a) Level diagram for S_{110}, with the splitting parameters α_3 and α_4 as predicted by the elastic-dipole model from the S_{100} and S_{111} experiment. The possible transitions between the levels by the quick (ν_q) and slow (ν_s) relaxation are indicated. (b) Level diagram as actually observed in the S_{110} experiment, with the proper α_3 parameters, but a strongly reduced effective $\bar{\alpha}_4$ parameter.

quantum motion, allowing dynamic studies in both regimes and tests on their interrelation with the static electric and elastic properties of the defects. Such a study and understanding of both regimes would supply an important model case for the rather unexplored question: Under which conditions will quantum motion take over at low temperatures in classical diffusion cases in solids.

As pointed out in Sec. I, the Ag^+ dipoles are not the only systems displaying the peculiar reorientation behavior discussed here. For the ⟨110⟩-reoriented N_2 defects in KCl and KI a similar supression of the 60° reorientation relative to the 90° effect was observed and qualitatively attributed to phonon dressing.[25] Several ⟨110⟩ off-center F^- defects and some ⟨110⟩ oriented OH^- molecules, which are presently under study[16–18] display a similar behavior in terms of their reorientation and/or elastic-dipole properties. The connection between the elastic dressing ($E_g > T_{2g}$) and the reorientation [$\tau(90°) > \tau(60°)$] properties of the Ag^+ defects treated here, may be therefore a model case for a whole group of ⟨110⟩-dipole defects.

D. α_4 discrepancy for RbBr : Ag^+ under S_{110}

The failure of the S_{110} experiment in RbBr : Ag^+ (Figs. 9 and 10) to yield an α_4 splitting parameter in agreement with the elastic-dipole relation $\alpha_4 = \frac{1}{2}\alpha_1 - \frac{3}{4}\alpha_2$ is a serious one in view of the quantitative agreement obtained for the same case in RbCl (Fig. 7) and the otherwise perfect consistency of all data with the elastic-dipole model. The simplest possibility for explaining such a discrepancy would be the assumption that—at least for certain stress directions—the elastic dipole does not behave as a "permanent" quantity, as assumed, but changes somewhat in magnitude or equilibrium orientation under stress. Attempts to explain in this way our S_{110} discrepancy fail, however, completely, for an evident reason: The measured stress and temperature dependence of the S_{110} effect (Figs. 9 and 10) follow perfectly the behavior for a *permanent and rigidly* ⟨110⟩*-oriented dipole with a fixed* (and *not* stress-dependent) α_4 value. The problem is that this α_4 value does not agree with the elastic-dipole relation $\alpha_4 = \frac{1}{2}\alpha_1 - \frac{3}{4}\alpha_2$. In Fig. 17 we illustrate this discrepancy in a level scheme drawn to scale: on the left-hand side (a) the S_{110} level splitting expected from the S_{100} and S_{111} experiments; on the right-hand side (b) the experimentally observed behavior, showing exactly the expected $\alpha_3 = \frac{3}{2}\alpha_2$ splitting, but a much too small α_4 splitting.

We cannot offer at this time any convincing explanation for this evident breakdown of the elastic-dipole model, though some initial efforts in this direction have been started. It should be noted that the α_4 splitting is different from all the other cases treated in one important aspect. The α_1, α_2, and α_3 parameters represent the splitting between dipole states of the *same symmetry* character: for the α_1 case (S_{100}) between E_g states, and for α_2 and α_3 (S_{111} and T_{2g}-part of S_{110}) between T_{2g} elastic-dipole states. The α_4 parameter represents the only case with a splitting between dipole states of *different* (E_g *and* T_{2g}) *symmetry*. We feel that this fact is somehwo responsible for the breakdown of the elastic-dipole picture. We note phenomenologically that [suggested by the effective-level diagram Fig. 17(b)] the observed α_4 value comes out numerically exactly right if we replace the proper elastic-dipole equation $\alpha_4 = \frac{1}{2}\alpha_1 - \frac{3}{4}\alpha_2$ by an *ad hoc* changed effective equation $\bar{\alpha}_4 = \frac{1}{2}\alpha_1 - \frac{3}{2}\alpha_2$.

Further discussions of this interesting breakdown of the elastic-dipole model and its possible explanations will be delayed until corresponding experimental material is available about other ⟨110⟩ defects with similar static and dynamic behavior, which are under study now. From the material available at this time it is already evident that a similar α_4 discrepancy appears in other dipole systems too, and therefore is not an isolated but a more general phenomena for ⟨110⟩ dipoles which must be taken serious.

ACKNOWLEDGMENT

The authors are indebted to B. G. Dick, A. S. Nowick, R. Pirc, L. Sander, and H. B. Shore for critical and helpful comments and suggestions in discussions and correspondence.

†Supported by NSF Grant No. GH43353X. Helium gas was provided by a departmental grant from ONR.
*Supported by a fellowship from ESFM-IPN, Mexico.

[1]S. Kapphan and F. Lüty, J. Phys. Chem. Solids 34, 969 (1973).
[2]V. Narayanamurti and R. O. Pohl, Rev. Mod. Phys. 42, 201 (1970).
[3]A. Gongora and F. Lüty, Solid State Commun. 14, 923 (1974); F. Lüty, Phys. Rev. B (to be published); H. U. Beyeler (unpublished).
[4]A. F. Devonshire, Proc. R. Soc. Lond. A 153, 601 (1936).
[5]R. J. Quigley and T. P. Das, Phys. Rev. 164, 1185 (1967).
[6]W. D. Wilson, R. D. Hatcher, R. Smoluchowski, and G. J. Dienes, Phys. Rev. 184, 844 (1969).
[7]R. J. Quigley and T. P. Das, Phys. Rev. B 7, 4004 (1973).
[8]W. Heinicke and F. Lüty, Bull. Am. Phys. Soc. 17, 143 (1972).
[9]R. J. Rollefson, Phys. Rev. B 5, 3235 (1972).
[10]S. Kapphan and F. Lüty, Phys. Rev. 6, 1537 (1972).
[11]H. U. Beyeler, Phys. Status Solidi 52, 419 (1972).
[12]P. Gosar and R. Pirc, in *Proceedings of the International Conference on Magnetic Research & Relaxation Ljubljana, Yugoslavia, Sept.* 1966, edited by R. Blinc (North-Holland, Amsterdam, 1968), p. 636; and R. Pirc and P. Gosar, Phys. Kondens. Mater. 9, 377 (1969).
[13]H. B. Shore, Phys. Rev. Lett. 17, 1142 (1966).
[14]The qualitative observation of stress optical effects, in agreement with a paraelastic alignment behavior, has been reported previously for these systems by W. Dultz [Proceedings of the International Conference on Phonons, Rennes 1971 (unpublished), p. 337]. No quantitative elastic-dipole values were derived in this work.
[15]H. B. Shore and L. M. Sander, following paper, Phys. Rev. B 12, 1546 (1975).
[16]R. Jimenez, S. Kapphan and F. Lüty (unpublished).
[17]A. Gongora and F. Lüty, International Conference on Color Centers, Sendai, 1974 (unpublished); and to be published.
[18]J. Wahl and F. Lüty (unpublished).
[19]A. S. Nowick and W. R. Heller, Adv. Phys. 12, 251 (1963).
[20]A preliminary report on these experimental results has been given in Bull. Am. Phys. Soc. 18, 304 A13 (1973).
[21]Ultrasonic measurements on the RbCl : Ag^+ system by Hallberg [Ph. D. thesis (Arizona State University, 1973) (unpublished)] yielded elastic-dipole moments which disagree with our values in magnitude, but agree roughly in terms of the ratio of the E_g and T_{2g} elastic-dipole part.
[22]In one of the most accurate quantitative investigations (with EPR on another ⟨110⟩ elastic-dipole system, the O_2^- molecule, by W. Känzig [J. Phys. Chem. Solids 23, 479 (1962)], the $\alpha_3 : \alpha_2$ ratio (which should be 1.5) yields, for instance, values of 1.16, 1.44, and 1.32 in three materials.
[23]W. Känzig, J. Phys. Chem. Solids 23, 479 (1962).
[24]The general case of a defect with two reorientation modes of very different rate, which cannot reach all of its equivalent states by the dominant process, is predicted and discussed in detail in the review paper by A. S. Nowick [Adv. Phys. 16, 1 (1967)]. Many of the discussed features, expected in general for such a defect, fit accurately our Ag^+ system, which seems to be the first well-established experimental example of such a behavior.
[25]R. H. Silsbee and I. Boiko, J. Phys. Chem. Solids 34, 1971 (1973).